One-dimensional gratings evolving through high-temperature annealing: sine-generated solutions

2012 J. Phys.: Condens. Matter 24 015001

(http://iopscience.iop.org/0953-8984/24/1/015001)

IOP PUBLISHING JOURNAL OF PHYSICS: CONDENSED MATTER

J. Phys.: Condens. Matter **24** (2012) 015001 (8pp) doi:10.1088/0953-8984/24/1/015001

One-dimensional gratings evolving through high-temperature annealing: sine-generated solutions

Marcos A Madrid, Roberto C Salvarezza and Marcos F Castez

Instituto de Investigaciones Fisicoquímicas Teóricas y Aplicadas (INIFTA), Casilla de Correo 16, Sucursal 4, (1900) La Plata, UNLP, CONICET, Argentina

E-mail: fcastez@inifta.unlp.edu.ar

Received 12 August 2011, in final form 31 October 2011
Published 17 November 2011
Online at stacks.iop.org/JPhysCM/24/015001

Abstract

Sine-generated curves (i.e. curves in which the curvature is a sine function of the arc-length parameter) have been used in the past to describe river meanders. Here we show how these curves spontaneously appear during the decay of high-aspect-ratio surfaces mediated by surface diffusion. We obtained analytical results for the kinetic evolution of such processes relevant to a wide class of initial geometries. Our theoretical results were satisfactorily compared with numerical simulations and with results from previous approaches to the same problem, and they can be useful for interpreting and designing experiments related to the technologically important process of high-temperature annealing on nano/micro-structured samples.

(Some figures may appear in colour only in the online journal)

1. Introduction

In the last few years, surface diffusion processes have attracted increasing interest in several branches of surface science, both from the theoretical and the experimental points of view [1–7, 9, 8, 28]. In particular, when high-temperature treatments are applied to solid samples, particle mobility is strongly enhanced, thus inducing important morphological modifications on them. Although different mechanisms, such as evaporation–condensation or bulk diffusion, can make a relevant contribution, in many cases, especially in nanoscale applications, surface diffusion is the most important mass-transport process.

Nanotechnology provides the ability to engineer the properties of materials by controlling their size and shape. In particular, anisotropic metallic and semiconductor nanostructures with high aspect ratios such as nanorods, nanowires, nanocolumns, nanoripples and flag-like nanocrystals have attracted considerable attention due to their unique physical properties. While the production of such nanostructures is in many cases a challenging task, shape control under temperature changes or even at room temperature is also an open issue with important practical implications. The knowledge of shape evolution under thermal treatments opens the possibility of predicting the viability or the lifetime of nanomaterial-based devices, or to produce new shapes, and accordingly new material properties, in a controlled way. In the last few years, thermal treatments have been widely used on semiconductor samples. Several technologically important applications of high-temperature hydrogen annealing in the semiconductor industry have been recently reported, thus becoming a very useful technique for obtaining devices with specific photonic or electronic properties. Hydrogen annealing has also been used on silicon substrates to reduce their surface roughness [14, 15], to round trench corners [16], to obtain special topologies [6, 17, 7], etc. Concerning the physical processes involved in the shape evolution of metals and semiconductors it is widely recognized that surface diffusion is the main factor operating at the nanoscale. This process is particularly important for metallic nanostructures that suffer drastic morphological changes at relatively low temperatures [10–12] and even at room temperature [13]. Regarding the theoretical interpretation of these applications of high-temperature hydrogen annealing

to change the morphological properties of semiconductor samples, it is worth remarking that such results have been properly interpreted in terms of the continuous theory of surface diffusion for isotropic materials [16, 18, 15, 19].

The continuous theory of interface evolution mediated by surface diffusion is a well-established topic since the pioneering work of Mullins [20, 21] and Herring [22]. In this framework, and under the assumption that all surface properties are independent of orientation, interface evolution is dictated by the Mullins equation:

$$v_{\mathrm{n}} = -K\Delta_{\mathrm{s}}\mathcal{C}, \tag{1}$$

where v_{n} is the normal velocity at a given point on the evolving surface, Δ_{s} is the intrinsic surface Laplacian (the so-called Laplace–Beltrami operator), and $\mathcal{C}$ is the local curvature. The coefficient K depends both on the type of material considered and on temperature through the relationship [20] $K = \frac{D_{\mathrm{s}}\gamma\Omega^2\nu}{k_{\mathrm{B}}T}$, where D_{s} is the diffusion constant, γ is the surface tension, Ω is the atomic volume, ν is the adatom density on the surface, k_{B} is the Boltzmann constant and T is the absolute temperature.

In a paper by Langbein and Leopold published in 1966 [23], sine-generated (SG) curves were introduced to describe the characteristic morphology of river meanders. A SG plane curve is one in which the angle θ between its tangent and a fixed axis (the x-axis, for instance), is a sine function of the arc-length parameter s. Thus, a SG curve can be written in an intrinsic way (i.e. in a way independent of the choice of the origin of coordinates), by means of the following relationship, that gives the angle θ as a function of the arc-length parameter (the so-called Whewell equation):

$$\theta(s) = R\sin\left(\frac{2\pi}{\lambda_{\mathrm{s}}}s\right), \tag{2}$$

where R and λ_{s} are the SG amplitude and wavelength respectively.

After the seminal paper by Langbein and Leopold [23], SG curves became a standard model to describe river meanders, widely employed in hydrology-related fields [24–26]. In this paper, we show how SG curves naturally appear in a very different context, specifically in the study of the surface-diffusion-driven decay of high-aspect-ratio (HAR)[1] patterned surfaces, but we also show the kinetic evolution of the parameters that describe the SG curve. Besides their relevance from the theoretical perspective, these results can be useful in practical and technological applications. Specifically, the results presented in this paper can be used to predict morphological properties and to obtain accurate estimations of annealing times in those applications in which a given HAR micro/nanopattern is submitted to high-temperature annealing [16, 6, 17, 7, 14].

The rest of the paper is organized as follows: the relevance of SG curves in the study of surface-diffusion-driven decay of 1D gratings and the basic geometrical properties of SG curves are discussed in section 2. Theoretical predictions about the time evolution of the parameters that characterize SG curves are shown in section 3, and these results are compared with numerical simulations in section 4. In section 5, we compare the results introduced in this paper with previous approaches to the same kind of problem. Finally, in section 6, we summarize our concluding remarks.

2. Emergence of SG curves in surface diffusion

As we mentioned before, in this work we combine and compare analytical and simulational results. Such simulations consist of a numerical integration of the Mullins equation, by means of which a plane curve restricted to periodic boundary conditions[2] evolves in a finite-difference scheme. Our numerical procedure supports dynamical regridding of the interface to overcome the numerical instabilities that often take place in those cases in which the aspect ratio of the initial interface is quite high.

To test the accuracy of our numerical scheme to obtain quantitative information for high-aspect-ratio interfaces, we have performed numerical simulations to compare with an analytical exact result published by Asvadurov *et al* [27]. In fact, these authors showed that the surface-diffusion-driven retraction of the tip of a wedge with angle of aperture 2Φ evolves in time as $\sim\delta(\Phi)t^{\frac{1}{4}}$. By means of an analytical study of similarity solutions in an analogue problem in the theory of curvature driven evaporation, Asvadurov *et al* found an exact result for the dependence of the coefficient δ with wedge aperture angle Φ (equation (3.24) in [27]). We have studied this dependence by numerically integrating the Mullins equation (1) for periodic triangular patterns (each triangle laying on a wedge of angle of aperture 2Φ) and measuring the retraction of the triangle tips for short times. These results are shown in figure 1, where the solid line represents the exact solution of Asvadurov *et al* [27] and the circles correspond to our numerical data. It is evident that simulational data fit very well with the analytical solution, thus showing that our numerical scheme gives accurate quantitative results even in cases of moderately high aspect ratios and also in the presence of quite sharp angles in the initial condition.

The spontaneous emergence of SG curves during the surface-diffusion-driven decay of 1D gratings can be readily seen in figure 2. In fact, figure 2(a) shows the shape adopted by an interface at successive times, starting from a rectangular HAR initial pattern, while figure 2(b) shows the dependence of the interface curvature as a function of the arc-length parameter for each of the interfaces shown in figure 2(a). From figure 2(b) it is clear that already at t_1, $\mathcal{C}(s)$ adopts a sinusoidal shape and it remains valid at later times, although the amplitude is time dependent and the wavelength of this sine curve decreases as time increases. Such a decrease in the wavelength is responsible for the fact that curves in figure 2(b)

[1] To be precise, we shall call the aspect ratio of a given 1D periodic pattern $\epsilon = \frac{W}{2\lambda}$, where W is the difference between the global maximum and minimum along the pattern and λ is its wavelength. Similarly, the ratio $\frac{W}{2}$ will be understood as the amplitude of such pattern.

[2] In real 3D systems, this geometry evidently applies to patterns invariant along a certain direction. Under this symmetry requisite, the interface is effectively one-dimensional.

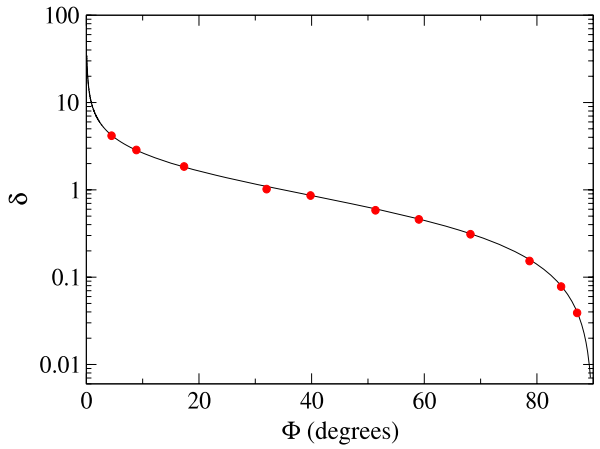

Figure 1. Solid line: dependence of coefficient δ as a function of Φ (where 2Φ is the aperture angle of the wedge), according to the exact result stated by equation (3.24) in [27]. Circles: δ versus Φ dependence, obtained by means of our finite-difference numerical integration of the Mullins equation.

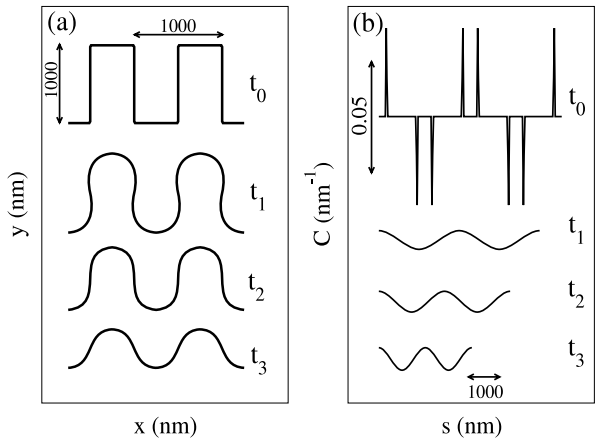

Figure 2. (a) An interface that initially (at $t = t_0$) is a HAR rectangular pattern evolves in a surface-diffusion-driven relaxation, adopting distinguishing shapes, as time increases ($t_0 < t_1 < t_2 < t_3$). (b) Curvature of the interface as a function of the arc-length parameter for each curve shown in (a).

become shorter as a function of time, which is a direct consequence of a general property of the surface diffusion flow of curves: it is length-shortening.

2.1. Basic geometrical aspects of SG curves

Let us discuss briefly a few general properties of SG curves. The periodic nature of SG curves becomes evident by its own definition (2). The typical shape of a SG curve of amplitude A is schematically drawn in figure 3. In equation (2), θ represents the angle between the positive direction of the x-axis and the tangent to the curve at a given point, R is the maximum value of this angle and λ_s is the arc-length in a period of the curve (length of the shadowed part in figure 3). When the arc-length parameter increases in a period, i.e. it increases from s to $s + \lambda_s$, the x-component increases from x to $x + \lambda_x$. Following the usual notation used in the

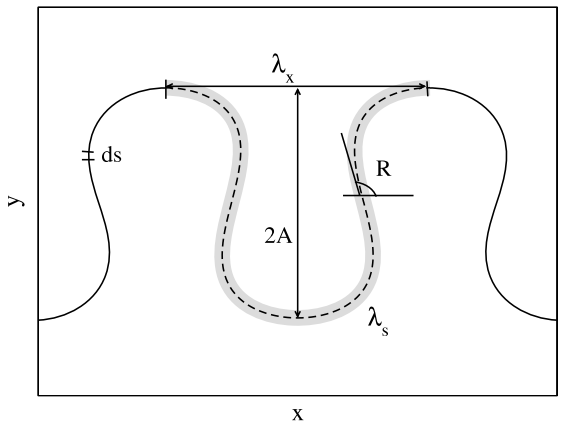

Figure 3. Sketch of a typical SG curve.

hydraulics-related literature [23–26], we shall call the ratio $\frac{\lambda_s}{\lambda_x}$ 'sinuosity'. The Whewell equation $\theta = \theta(s)$ implies the following differential forms for the x and y components:

$$\mathrm{d}x = \cos(\theta(s))\,\mathrm{d}s \tag{3}$$

$$\mathrm{d}y = \sin(\theta(s))\,\mathrm{d}s. \tag{4}$$

Combining equation (3) with the Whewell equation $\theta(s) = R\sin(k_s s)$ (where $k_s = \frac{2\pi}{\lambda_s}$) for a SG curve it can be seen that $\frac{\mathrm{d}x}{\mathrm{d}s} \geq 0$ if $0 \leq R \leq \frac{\pi}{2}$. When the parameter R is higher than $\frac{\pi}{2}$, the x-component is not monotonically increasing, thus the resulting SG curve becomes multivalued (i.e. in that case the SG curve is not the graph of a function $y(x)$), as is the case for the SG curve shown in figure 3. Qualitatively speaking, the same shape remains for values of R in the range $\frac{\pi}{2} < R < \sim 2.11$. However, for values of R higher than ~ 2.11, the SG curve self-intercepts, leading to non-physical curves (associating curves with interfaces). In this paper we shall only consider physically realistic SG curves, thus throughout this paper we will assume that $0 \leq R < \sim 2.11$.

From differential forms (3) and (4), we can immediately obtain parametric equations for the x and y components as functions of the arc-length parameter s for a SG curve:

$$x(s) = \int_0^s \cos\left(R\sin\left(\frac{2\pi}{\lambda_s}u\right)\right)\mathrm{d}u + x_0 \tag{5}$$

and

$$y(s) = \int_0^s \sin\left(R\sin\left(\frac{2\pi}{\lambda_s}u\right)\right)\mathrm{d}u + y_0. \tag{6}$$

We can obtain λ_x (defined in figure 3) as a function of parameters R and λ_s, evaluating the integral on the right side of (5) for $s = \lambda_s$:

$$\lambda_x = \int_0^{\lambda_s} \cos\left(R\sin\left(\frac{2\pi}{\lambda_s}u\right)\right)\mathrm{d}u. \tag{7}$$

Performing a simple substitution and using a well-known integral representation of Bessel functions [29], we obtain

$$\lambda_x = \lambda_s J_0(R), \tag{8}$$

where J_0 is the Bessel function of the first kind and order zero. Equation (8) implies that the sinuosity (σ) of a SG curve

depends on R through the relationship

$$\sigma = \frac{\lambda_s}{\lambda_x} = \frac{1}{J_0(R)}. \tag{9}$$

Similarly, making $s = \frac{\lambda_s}{2}$ in (6), we can find an exact result for the amplitude A of a SG curve. In fact, after a change of variables, we obtain

$$A = \frac{\lambda_s}{4\pi} \int_0^{\pi} \sin(R\sin(u))\,\mathrm{d}u. \tag{10}$$

The integral on the right-hand side of (10) can be written in terms of the so-called Struve function [30]:

$$A = \frac{\lambda_s}{4} H_0(R), \tag{11}$$

where $H_0(R)$ is the zero-order Struve function (notice that $H_0(R) > 0$ for the considered values of R, i.e. those in the range $[0, \sim 2.11]$). Combining (9) and (11) we obtain a closed form for the aspect ratio of a SG curve:

$$\epsilon(R) = \frac{H_0(R)}{4J_0(R)}. \tag{12}$$

It is worth noticing that equation (12) shows us that ϵ depends on R, but it is independent from λ_s, so for any fixed value of λ_x, the value of the amplitude R defines the shape of the SG curve.

3. Time evolution of the parameters: theoretical predictions

As shown in section 2 (see figure 2), SG curves spontaneously emerge during the surface-diffusion-driven decay of 1D HAR gratings. Thus, it is natural to study time-dependent SG curves in the form

$$\theta(t, s) = R(t)\sin\left(\frac{2\pi}{\lambda_s(t)}s\right). \tag{13}$$

However, irrespective of the choice of functions $R(t)$ and $\lambda_s(t)$, such time-dependent SG curves are not exact solutions of the Mullins equation (this can be easily demonstrated by introducing expression (13) into the Mullins equation written out in terms of $\theta(t, s)$, equation (1.8) in [27]). However, our numerical simulations (figure 2, for instance) tell us that such expressions should be good approximations to the true solutions. Therefore, we will attempt to find the functions $R(t)$ and $\lambda_s(t)$ to obtain a closed form for these approximated solutions. To accomplish this task, we will evidently need two relationships involving $R(t)$ and $\lambda_s(t)$ in the surface diffusion flow. One of these relationships is provided by the imposed boundary conditions: in fact, we are looking for periodic solutions for the surface diffusion flow, in which λ_x is constant (it does not change with time). Therefore, equation (9) tells us that knowing the time dependence of the amplitude $R(t)$ it suffices to know the time dependence of $\lambda_s(t)$:

$$\lambda_s(t) = \frac{\lambda_x}{J_0(R(t))}. \tag{14}$$

An immediate consequence of the Mullins equation is that the total length of the interface satisfies the following relationship [31]:

$$\frac{\mathrm{d}L(t)}{\mathrm{d}t} = -K\int_{L(t)} \mathcal{C}_s^2\,\mathrm{d}s, \tag{15}$$

where $L(t)$ is the total length of the curve[3]. Evaluating (15) for a period of a SG curve (using that $\mathcal{C} = \theta_s$), we obtain

$$\frac{\mathrm{d}\lambda_s(t)}{\mathrm{d}t} = -8K\pi^4\frac{R^2(t)}{\lambda_s^3(t)}. \tag{16}$$

Differentiating (14) and combining it with (16) we can eliminate $\lambda_s(t)$ from such equations and thus we obtain a closed form evolution equation for the amplitude $R(t)$:

$$\frac{\mathrm{d}R}{\mathrm{d}t} = -K\frac{(2\pi)^4}{\lambda_x^4}R^2\frac{J_0^5(R)}{2J_1(R)}. \tag{17}$$

The pair of equations (14) and (17) constitute a closed set of equations giving us a theoretical prediction that fully determines the SG solution (13) at any given time, under the assumption that the curve keeps its SG shape during the whole decaying process. In section 4 we will check the accuracy of this theoretical prediction, contrasting it with numerical simulations.

4. Numerical results

In the first place, we contrasted our theoretical predictions against a direct numerical integration of the Mullins equation in cases in which the initial condition is a SG curve. In this sense, figure 4 shows the time evolution for both the aspect ratio ϵ and the arc-length in a period of the interface λ_s (notice that knowing ϵ at any time we can find the associated value for $R(t)$ by using (12), that is an invertible relationship in the range considered for the parameter R), starting from SG curves with different initial values for the parameter R (i.e. we are considering SG curves with different sinuosity at the initial state). Figure 4 shows an excellent agreement between numerical simulations (solid lines) and theoretical expectations (dotted lines) for all considered values of R_{ini}, since it is almost impossible to distinguish with the naked eye between related curves obtained from both approaches. Remarkably, these results show that the pair of equations (14) and (17) account very accurately for the surface-diffusion-driven decay of SG curves with aspect ratios in the range $[0, \sim 1]$, thus largely increasing the range of accuracy of the linear theory of surface diffusion, that ordinarily is restricted to the range $0 \leq \epsilon \leq \sim 0.1$. Once the values of $R(t)$ and $\lambda_s(t)$ are known we can, by employing (2), reconstruct the SG interface. Although, as we pointed out above, theoretical values for $R(t)$ and $\lambda_s(t)$ are in excellent agreement with numerical simulations, one might ask if small errors in values of $R(t)$ and/or $\lambda_s(t)$ could lead to some observable difference in the associated SG curve. Therefore,

[3] As the second member in (15) is non-positive, that equation proves that the surface diffusion flow is area-decreasing (length-decreasing in the 1D case).

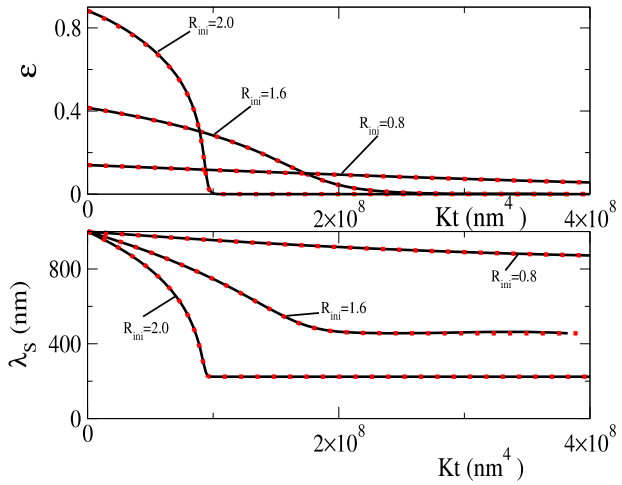

Figure 4. Dependences of ϵ (at the top) and λ_s (at the bottom) with the (rescaled) time Kt, for a SG initial condition with $\lambda_{s_{ini}} = 1000$ nm and several different values of the initial amplitude R_{ini}. Solid lines correspond to numerical simulations and dotted lines are the expected theoretical values according to (14) and (17).

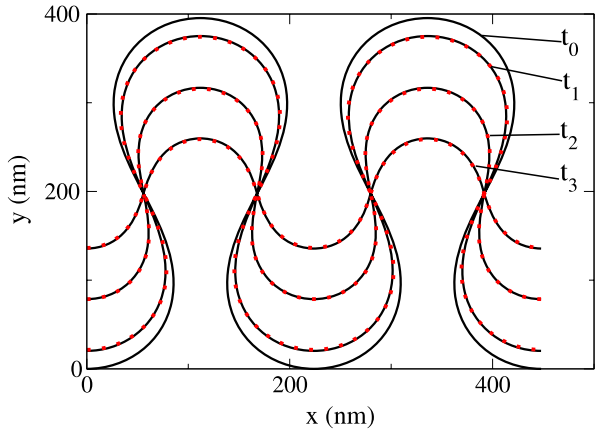

Figure 5. Interface shapes at successive times ($t_0 < t_1 < t_2 < t_3$), for a SG initial condition (curve that corresponds to t_0). Solid lines were obtained by a numerical integration of the Mullins equation, while dotted lines were reconstructed by using the analytical prediction for the time dependence of $R(t)$ and $\lambda_s(t)$, according to equations (14) and (17).

we should compare the predicted theoretical interface against the simulated one. That comparison was performed and the results are shown in figure 5. In fact, solid lines in figure 5 correspond to a numerical integration of the Mullins equation for the initial condition labelled as t_0, while dotted lines correspond to the interfaces predicted (at three successive values of time $t_1 < t_2 < t_3$) by using equations (14) and (17). Figure 5 shows that, at any time, the agreement between simulated interfaces and the theoretical ones is excellent, since also in this case the associated interfaces are almost indistinguishable.

Up to now, we have shown how the pair of equations (14) and (17) provides an excellent approximation for the time evolution of the surface-diffusion-driven decay process when the initial interface is a SG curve. Evidently, thinking of applications to real situations, is necessary to analyse how

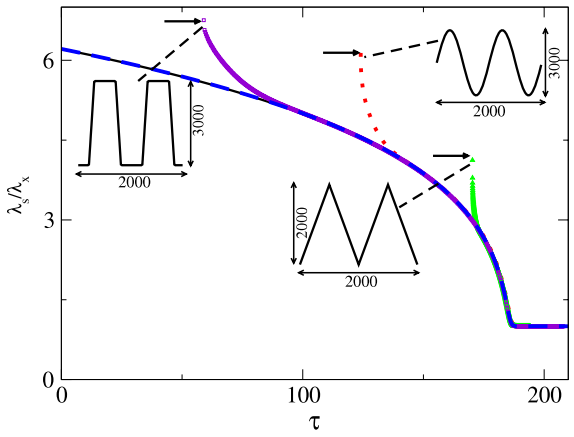

Figure 6. Dependence of the ratio $\frac{\lambda_s}{\lambda_x}$ on the dimensionless time τ. The solid line correspond to a SG curve with $R = 2.11$ as the initial condition, while the dashed line is the theoretical prediction according to (14) and (17). Remaining curves correspond to initial conditions indicated inside the graph. Horizontal arrows are used to indicate that curves were shifted along the τ axis, to obtain data-collapse.

these results apply to more general initial conditions. As we discussed in section 2, we found that for a broad class of patterns an initially non-SG grating decays, after a transient time (see figure 2), into a SG curve. This means that our results for SG curves are applicable to a broad class of initial patterns, once such transient time has elapsed[4]. In this sense, it is expected that time-dependent pattern characteristics converge, after a first transient stage, towards the dependence found for SG patterns. Figure 6 shows this behaviour for the ratio $\frac{\lambda_s}{\lambda_x}$ as a function of the dimensionless time defined as $\tau = (\frac{2\pi}{\lambda_x})^4 Kt$. In fact, the solid line in figure 6 corresponds to a SG curve with $R = 2.11$ as the initial condition in a numerical simulation, the dashed line is the theoretical prediction according to equations (14) and (17) (both curves are almost coincident), while the remaining curves correspond to numerical simulations for several classes of HAR patterns (indicated inside the graph) as initial conditions. To overcome the existence of a different transient time for each case, curves associated with non-SG initial conditions were shifted along the τ axis (indicated by horizontal arrows in figure 6), to obtain data-collapse with the SG solution. As becomes evident by the analysis of figure 6, for a broad class of HAR initial patterns (trapezoidal, sinusoidal, triangular, etc) the kinetic behaviour of observable quantities (such as the sinuosity $\frac{\lambda_s}{\lambda_x}$) follows (beyond the transient stage) the same dependency found for SG patterns.

The fact that a given HAR pattern (e.g. a rectangular HAR pattern) decays after a transient time into a SG curve can be viewed, from the perspective of its harmonic content, as a fast filtering of short wavelength Fourier modes in the same way as occurs in the linear limit of the Mullins equation. In fact, it is well known that in such a limit, Fourier modes

[4] The exact elapsed time in the transient stage evidently depends on the specific pattern and we won't discuss that in this paper, although obtaining at least an estimated value could be important in practical situations.

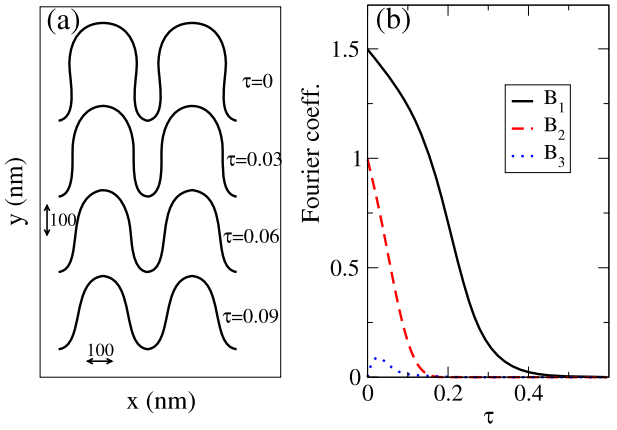

Figure 7. (a) Snapshots, at successive times, showing the relaxation of an initial condition that is a generalized SG curve, with two Fourier components in its Whewell equation $\theta(s) = B_1 \sin(k_s s) + B_2 \sin(2k_s s)$. (b) Time evolution of the first three spectral components of the interface. Values of the parameters in the initial condition are $B_1 = 1.5$, $B_2 = 1.0$ and $k_s = \frac{2\pi}{1000}$ nm^{-1}.

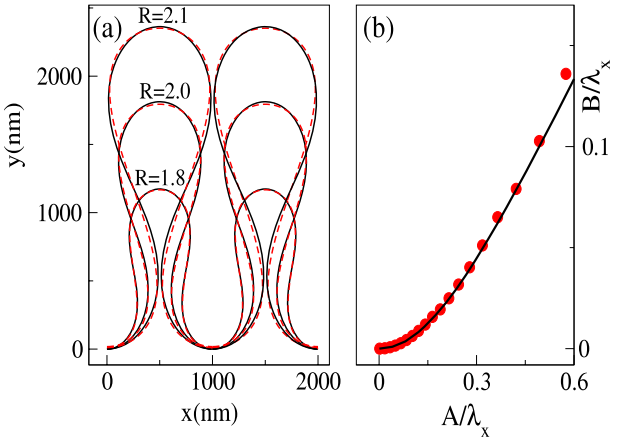

Figure 8. (a) SG curves for different values of R (solid lines) and the associated parametric curves defined in (19) with parameters fitted trying to minimize the area enclosed by the curves (dashed lines). (b) (Solid line) asymptotic trajectory in $(\epsilon = \frac{A}{\lambda_x}, \frac{B}{\lambda_x})$ phase space according to equation (22) in [34]. (Circles) Points in the plane $(\epsilon, \frac{B}{\lambda_x})$ obtained by fitting parametric curves to SG curves with different values of R.

decay exponentially with time and with a lifetime that depends on wavelength as λ_x^4. However, beyond this linear limit, the Mullins equation is nonlinear; thus linear superposition ideas are not applicable. Therefore, it is interesting to study the time evolution of Fourier coefficients for a typical pattern during the decay process. In fact, let us suppose that, at time t, such a pattern is described by $\theta(s, t)$. For a fixed value of t, θ is a periodic function of s of wavelength $\lambda_s(t)$. Therefore, it can be expanded in a standard Fourier series

$$\theta(s,t) = \frac{A_0}{2} + \sum_{n=1}^{\infty} \left(A_n(t) \cos\left(\frac{2\pi}{\lambda_s(t)} ns\right) + B_n(t) \sin\left(\frac{2\pi}{\lambda_s(t)} ns\right)\right). \quad (18)$$

To study the time evolution of coefficients A_n and B_n in a typical situation, we have performed a numerical simulation of the decay process starting from an initial condition in which $B_1 = 1.5$, $B_2 = 1.0$ and the rest of the Fourier coefficients were taken equal to zero, and Fourier coefficients were numerically computed during the whole decay process. Interface shapes at different times are shown in figure 7(a), while the time evolution of the main Fourier coefficients is shown in figure 7(b) (the rest of the computed coefficients became negligible). We can see in figure 7(b) how the component B_3, absent in the initial condition, spontaneously appears, although it decays after a short transient. This emergence of higher order harmonics is evidently a nonlinear effect, since it has no room within the linear theory. Figure 7(b) also shows that already for $\tau = \sim 0.1$, the B_1 component is the main contribution, i.e. at that time the interface is nearly a SG curve. Notice that this occurs even when the initial condition (figure 7(a), $\tau = 0$) does not have the peak–valley symmetry property present in SG curves. Therefore, the ideas presented in this paper can, in principle, be applied to initial patterns without such peak–valley symmetry, although it becomes evident that the time elapsed in the transient stage will grow as this asymmetry increases.

5. Relation to previous approaches

In a series of recent papers [32–35], some of the authors of this work studied the surface-diffusion-driven decay of HAR patterns by employing a different class of curves than SG ones. In fact, the typical shape of a SG curve (see figure 3) can be reproduced, within an excellent approximation, with a simple explicit parametric expression depending on two time-dependent coefficients A and B:

$$(x(p,t), y(p,t)) = \left(p - B(t) \sin\left(2\frac{2\pi}{\lambda_x} p\right), A(t) \sin\left(\frac{2\pi}{\lambda_x} p\right)\right), \quad (19)$$

where p is a parameter that has length units and takes values in the range $[0, L_s]$ and L_s is the pattern length.

For low values of the sinuosity of the curves (i.e. low values of R), a pair of values of parameters (A, B) can be found such that the SG and parametric curves become almost indistinguishable. This can be seen in figure 8(a), where we have plotted SG curves for several values of the SG amplitude R and, by means of an optimization procedure based on the minimization of the enclosed area, we have found the values of parameters (A, B) giving the best fitting. We can see that a very good fit can be obtained even for the highest considered value of the SG amplitude ($R = 2.1$), that is almost in the self-crossing limit of the curve.

One of the most distinguishable facts considering the time evolution of the decay process in those previous studies is that trajectories starting from an arbitrary point in the (A, B) phase space quickly approximate a special trajectory [34, 35]. In [34] an analytical ad hoc approximation for such a special trajectory was proposed (see equation (22) in [34]). Although

the existence of such an asymptotic trajectory was supported by numerical simulations and is consistent with experimental data [35], the origin of such behaviour remained obscure. However, we will show that under the SG based approach presented in this paper, the origin of such behaviour can be explained. Indeed, if we look at figure 8(b) we can see that the solid line represents the asymptotic curve obtained with the ad hoc expression in equation (22) of [34], while circles in figure 8 are associated with data obtained by taking the (A, B) values corresponding to different amplitudes R according to the optimization procedure described above. Thus, the conclusion becomes evident: the 'asymptotic' trajectory in (A, B) space is the one that makes the parametric function (19) adopt a (in a good approximation) SG shape.

So, the description of the particular behaviour found in the previous description using parametric functions (19) becomes much simpler (and thus more natural) under the SG framework. The idea of a pair of parameters (A, B) approaching a special trajectory can be restated in a simpler way: once the transient stage has elapsed, patterns adopt a SG shape characterized by a single parameter R (of course, pattern wavelength λ_x is an additional parameter in both approaches).

6. Summary and concluding remarks

We have shown how SG curves spontaneously emerge during the decay of HAR 1D gratings mediated by surface diffusion. We proposed analytical solutions in the form of SG curves with time-dependent amplitude and wavelength and we found analytical expressions for such time dependences. Although these expressions are not exact solutions of the Mullins equation, they are, according to our numerical simulations, excellent approximations to such exact solutions over the full range of amplitudes considered, that is the range in which SG curves can describe physically realistic interfaces. Such a range is well beyond the scope of the linear theory of surface diffusion, thus our results can be applied to situations, as in the case of the decay of HAR gratings, where the linear theory of surface diffusion is not applicable.

By means of the obtained theoretical approximation we can predict, with great accuracy, the shape adopted for an initially SG curve at any time during the decay process. Moreover, we have shown how this solution is also relevant for a broad class of initial HAR gratings (different from the SG ones), in the sense that after a short transient time (that depends on the exact geometry of the initial condition), the kinetic evolution of such systems converges into that corresponding to SG curves, for which our theoretical solution represents an excellent approximation.

On the other hand, we have compared our results with a previous approach to the same problem (approach based on the use of another family of curves different from the SG), introduced recently by one of us [34]. As a conclusion of this comparison, it becomes evident that the framework introduced in this paper (based on SG curves) is more robust and natural, in the sense that it provides much more accurate predictions for the time evolution of measurable quantities such as pattern amplitudes or surface areas. Although the previous approach [34] has the advantage of giving an accurate description of morphological aspects by means of simple parametric equations, its accuracy regarding the time evolution of the system is rather poor and quickly deteriorates when the aspect ratio increases. On the other hand, some relationships that were numerically found (with no analytical support) in the previous approach, appear naturally under the present description based on SG curves. The development of an accurate mathematical tool to describe shape evolution of HAR nanostructures is certainly a valuable contribution, considering possible applications in nanoscience and nanotechnology. In fact, this tool can be useful to predict the viability or the lifetime of a variety of nanomaterial-based devices that use this type of structure, or to produce materials with new shapes, and accordingly with new properties, by simply tuning the surface mobility.

Acknowledgments

This work has been accomplished as part of the projects PICT 06-621 and PICT 2010-1921 of ANPCyT (Argentina). RCS and MFC are members of CONICET (the Argentina National Research Council).

References

[1] Malshe R, Ediger M D, Yu L and de Pablo J J 2011 Evolution of glassy gratings with variable aspect ratios under surface diffusion *J. Chem. Phys.* **134** 194704
[2] Erlebacher J, Aziz M J, Chason E, Sinclair M B and Floro J A 2000 Nonclassical smoothening of nanoscale surface corrugations *Phys. Rev. Lett.* **84** 5800
[3] Combe N, Jensen P and Pimpinelli A 2000 Changing shapes in the nanoworld *Phys. Rev. Lett.* **85** 110
[4] Ramana Murty M V 2000 Morphological stability of nanostructures *Phys. Rev.* B **62** 17004–11
[5] Bonzel H P and Preuss E 1995 *Surf. Sci.* **336** 209
[6] Bopp M, Coronel P, Bustos J, Pribat C, Dainesi P, Skotnicki T and Ionescu A M 2009 Silicon nanostructuring for 3d bulk silicon versatile devices *Microelectron. Eng.* **86** 885–8
[7] Lee M-C M, Chiu W-C, Yang T-M and Chen C-H 2007 Monolithically integrated low-loss silicon photonic wires and three-dimensional tapered couplers fabricated by self-profile transformation *Appl. Phys. Lett.* **91** 191114
[8] dos Santos Claro P C, Castez M F, Schilardi P L, Luque N B, Leiva E P M and Salvarezza R C 2008 Spontaneous nanoripple formation on metallic templates *ACS Nano* **12** 2531–9
[9] Castez M F and Albano E V 2009 Continuous and discrete modeling of the decay of two-dimensional nanostructures *J. Phys.: Condens. Matter* **21** 263001
[10] Karim S, Toimil-Molares M E, Balogh A G, Ensinger W, Cornelius T W, Khan E U and Neumann R 2006 Morphological evolution of au nanowires controlled by Rayleigh instability *Nanotechnology* **17** 5954–9
[11] Bracco G and Cavanna D 2007 Decay of nanoripples on Au(111) studied by he atom scattering *Phys. Rev.* B **76** 033411
[12] Toimil Molares M E, Balogh A G, Cornelius T W, Neumann R and Trautmann C 2004 Fragmentation of nanowires driven by Rayleigh instability *Appl. Phys. Lett.* **85** 5337–9

[13] Sun Y, Mayers B and Xia Y 2003 Transformation of silver nanospheres into nanobelts and triangular nanoplates through a thermal process *Nano Lett.* **3** 675
[14] Hiruta R, Kuribayashi H, Shimizu S, Sudoh K and Iwasaki H 2004 Evolution of surface morphology of Si-trench sidewalls during hydrogen annealing *Appl. Surf. Sci.* **237** 63–7
[15] Lee M-C M and Wu M C 2006 Thermal annealing in hydrogen for 3-D profile transformation on silicon-on-insulator and sidewall roughness reduction *J. Microelectromech. Syst.* **15** 338–43
[16] Nakamura J, Sudoh K and Iwasaki H 2007 Evolution of one-dimensional gratings with high aspect ratios on Si(001) surfaces by high-temperature annealing *Japan. J. Appl. Phys.* **46** 7194–7
[17] Mizushima I, Sato T, Taniguchi S and Tsunashima Y 2000 Empty-space-in-silicon technique for fabricating a silicon-on-nothing structure *Appl. Phys. Lett.* **77** 3290–2
[18] Sudoh K, Iwasaki H, Hiruta R, Kuribayashi H and Shimizu R 2009 Void shape evolution and formation of silicon-on-nothing structures during hydrogen annealing of hole arrays on Si(001) *J. Appl. Phys.* **105** 083536
[19] Sudoh K, Iwasaki H, Kuribayashi H, Hiruta R and Shimizu R 2004 Numerical study on shape transformation of silicon trenches by high-temperature hydrogen annealing *Japan. J. Appl. Phys.* **43** 5937–41
[20] Mullins W W 1957 Theory of thermal grooving *J. Appl. Phys.* **28** 333
[21] Mullins W W 1959 Flattening of a nearly planar solid surface due to capillarity *J. Appl. Phys.* **30** 77
[22] Herring C 1951 *Physics of Powder Metallurgy* ed W E Kingston (New York: McGraw-Hill)
[23] Leopold L B and Langbein W B 1966 River meanders *Sci. Am.* **214** 60–70
[24] Langbein W B and Leopold L B 1966 River meanders: theory of minimum variance *United States Geological Survey Professional Paper* **422-H** 1–15
[25] Hayes B 2006 Up a lazy river *Am. Sci.* **94** 490–4
[26] Ferreira Da Silva A M 2006 On why and how do rivers meander *J. Hydraul. Res.* **44** 579–90
[27] Asvadurov S, Coleman B D, Falk R S and Moakher M 1998 Similarity solutions in the theory of curvature driven diffusion along planar curves: I. Symmetric curves expanding in time *Physica* D **121** 263–74
[28] Castez M F, dos Santos Claro P C, Schilardi P L, Andreasen G and Salvarezza R C 2010 Surface relaxation of high-aspect-ratio nanostructures: theory and experiments *J. Phys. Chem.* C **114** 4603–10
[29] Abramowitz M and Stegun I A 1972 *Handbook of Mathematical Functions* tenth printing (New York: Dover) p 360
[30] Abramowitz M and Stegun I A 1972 *Handbook of Mathematical Functions* tenth printing (New York: Dover) pp 496–9
[31] Mayer U F 2001 Numerical solutions for the surface diffusion flow in three space dimensions *Comput. Appl. Math.* **20** 361–79
[32] Castez M F and Salvarezza R C 2009 Modeling thermal decay of high-aspect-ratio nanostructures *Appl. Phys. Lett.* **94** 053103
[33] Castez M F 2010 Generalized Fourier analysis for nanopatterns with overhangs *Europhys. Lett.* **89** 28001
[34] Castez M F 2010 Surface-diffusion-driven decay of patterns: beyond the small slopes approximation *J. Phys.: Condens. Matter* **22** 345007
[35] Castez M F, Salvarezza R C, Nakamura J and Sudoh K 2010 A theoretical framework to obtain interface's shapes during the high-temperature annealing of high-aspect-ratio gratings *Appl. Phys. Lett.* **97** 123104